Palaeogeography, Palaeoclimatology, Palaeoecology 601 (2022) 111128

Contents lists available at ScienceDirect

Palaeogeography, Palaeoclimatology, Palaeoecology

journal homepage: www.elsevier.com/locate/palaeo

Identification, characterization, and paleoclimatic implication of Early Cretaceous (Aptian-Albian) paleosol succession in Zhangye Danxia National Geopark, northwestern China

Xuegang Mao [a,b,*], Gregory Retallack [c], Xiuming Liu [a,b,d]

[a] Institute of Geography, Fujian Normal University, Fuzhou 350007, China
[b] State Key Laboratory of Subtropical Mountain Ecology (Funded by Ministry of Science and Technology and Fujian Province), Fujian Normal University, Fuzhou 350007, China
[c] Department of Earth Science, University of Oregon, Eugene, Oregon 97403-1272, USA
[d] Department of Earth and Environmental Sciences, Macquarie University, Sydney, NSW 2109, Australia

ARTICLE INFO

Editor: Howard Falcon-Lang

Keywords:
Pedotypes
Pedogensis
Soil horizon
Carbonate content
Paleoenvironment

ABSTRACT

Paleosols are useful evidence of paleoclimates and paleoenvironments independent of fossils. Zhangye Danxia National Geopark of Gansu Province (northwestern China) has been protected for its stunning varicolored badlands of Early Cretaceous (Aptian-Albian) claystones. However, the paleoclimates and paleoenvironments forming such unique succession are currently not well understood. The widespread pedogenic features, for example root traces and soil horizons, indicate different paleosols, which provides clues of associated paleoclimates and paleoenvironments. In the present study, combining field work and soil micromorphology, we recognized, classified, and interpreted 155 sequential paleosol profiles of 14 different pedotypes (soil types) in the 755-m-thick section. These pedotypes have modern analogues in South Asia, indicating hotter and more humid paleoclimate than at present in Zhangye. Systematic analysis of soil units based on comparison to their modern analogues allows reconstruction of paleoenvironments in eleven humidity stages. Variation in waterlogging of the paleosols based on the ratio of Hm / Gt agreed well with regional and global paleoclimatic records, confirming its utility in paleoclimate reconstruction during Aptian and Albian. The identification and characterization of the paleosol succession provides a significant base for detailed paleoclimatic reconstruction during this period.

1. Introduction

The Cretaceous has been considered a time of greenhouse climate (Ogg et al., 2016), and as a guide to modern and future global warming (Hay, 2017; Zachos et al., 2008). Cretaceous sediments including continental red beds (Huang et al., 2012; Wang et al., 2013), organic-rich black shales (Jenkyns, 2010; Leckie et al., 2002; Li et al., 2020), and Cretaceous oceanic red beds (CORBs) (Hu et al., 2012; Wang et al., 2011) have been investigated to reconstruct the Cretaceous paleoclimate and paleoenvironment. In northwestern and northeastern China, paleosols are widespread in Cretaceous continental sediments, and are receiving increasing attention for paleoclimatic reconstruction (Huang et al., 2012; Li et al., 2016; Wang et al., 2013).

Paleosols are ancient soils incorporated within the geological record, and provide important archives for reconstructing paleoclimate and paleoenvironment both qualitatively and quantitatively (Sheldon and Tabor, 2009; Tabor and Myers, 2015). Some qualitative reconstructions of paleoclimate are based on paleosol taxonomy compared to their modern analogues and sequence stratigraphic approaches (Kraus, 1999; Retallack et al., 2000), but quantitative reconstructions rely on geochemical and morphological relationships with environmental parameters deduced from modern soil datasets (Sheldon and Tabor, 2009; Tabor and Myers, 2015). In any case, the first step is recognizing and characterizing paleosols. Soil formation is a process of altering and redistributing parent materials physically and chemically. Soil or paleosol features can be distinguished from sedimentary structures in field, by micromorphology, and by geochemistry (Brewer, 1976; Fitzpatrick, 1984; Retallack, 2016). The most important field criterion for paleosols geologically younger than Silurian is root traces, but soil horizons and soil structures also are distinctive in the field for those familiar with

* Corresponding author at: Institute of Geography, Fujian Normal University, Fuzhou 350007, China.
E-mail addresses: maoxuegang1@163.com (X. Mao), gregr@uoregon.edu (G. Retallack), xliu@fjnu.edu.cn (X. Liu).

https://doi.org/10.1016/j.palaeo.2022.111128
Received 18 December 2020; Received in revised form 13 June 2022; Accepted 19 June 2022
Available online 25 June 2022

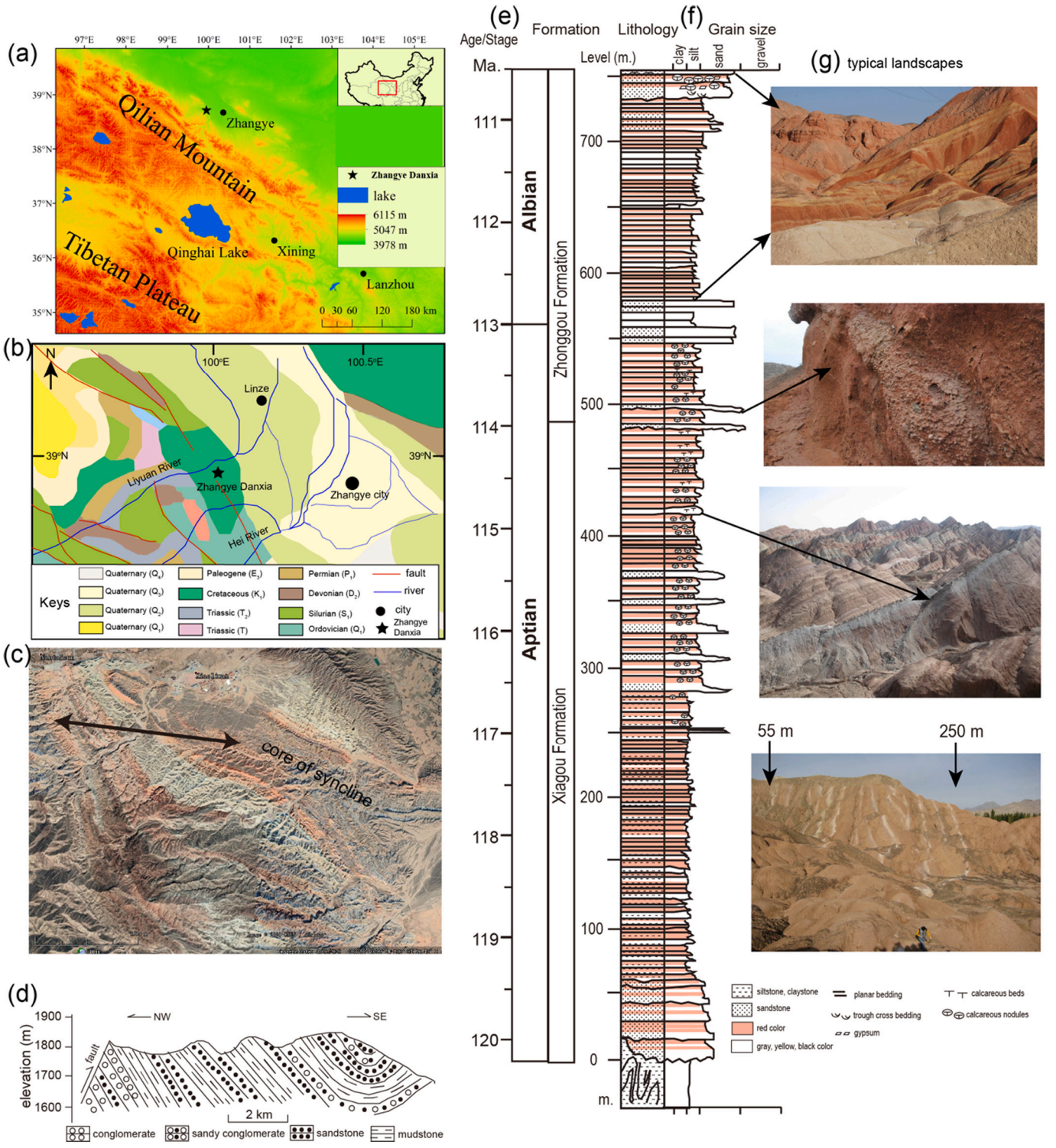

Fig. 1. Study area and geological settings. (a) location of Zhangye Danxia National Geopark. (b) geological map of Zhangye basin (modified after www.ngac.org.cn). (c) Google image of Zhangye Danxia National Geopark. (d) schematic cross-section of Zhangye Danxia National Geopark (after Ding et al. (2014)). (e) age and formation of Zhangye Danxia section (modified after Liu et al. (2017)). (f) lithological stratigraphy of Zhangye Danxia section mapped in field. (g) representative field photos at specific stratigraphic levels.

modern soils.

The Early Cretaceous (Aptian-Albian) paleosol succession of Zhangye Danxia Geopark in northwestern China is exceptional for multicolored hue and bed cyclicity (Liu et al., 2017). Pedogenic features, such as root traces, carbonate nodules, soil horizons, are ubiquitous in Zhangye Danxia section, undocumented until now. In the present study, paleosols in Zhangye Danxia section were identified, classified and characterized by field observations and micromorphology. Each pedotype was described and interpreted within a stratigraphic section of Zhangye Danxia as first step to reconstruct paleoclimatic and paleoenvironmental times series. This qualitative assessment of humidity/aridity variation from paleosol interpretation has both regional and global paleoclimatic

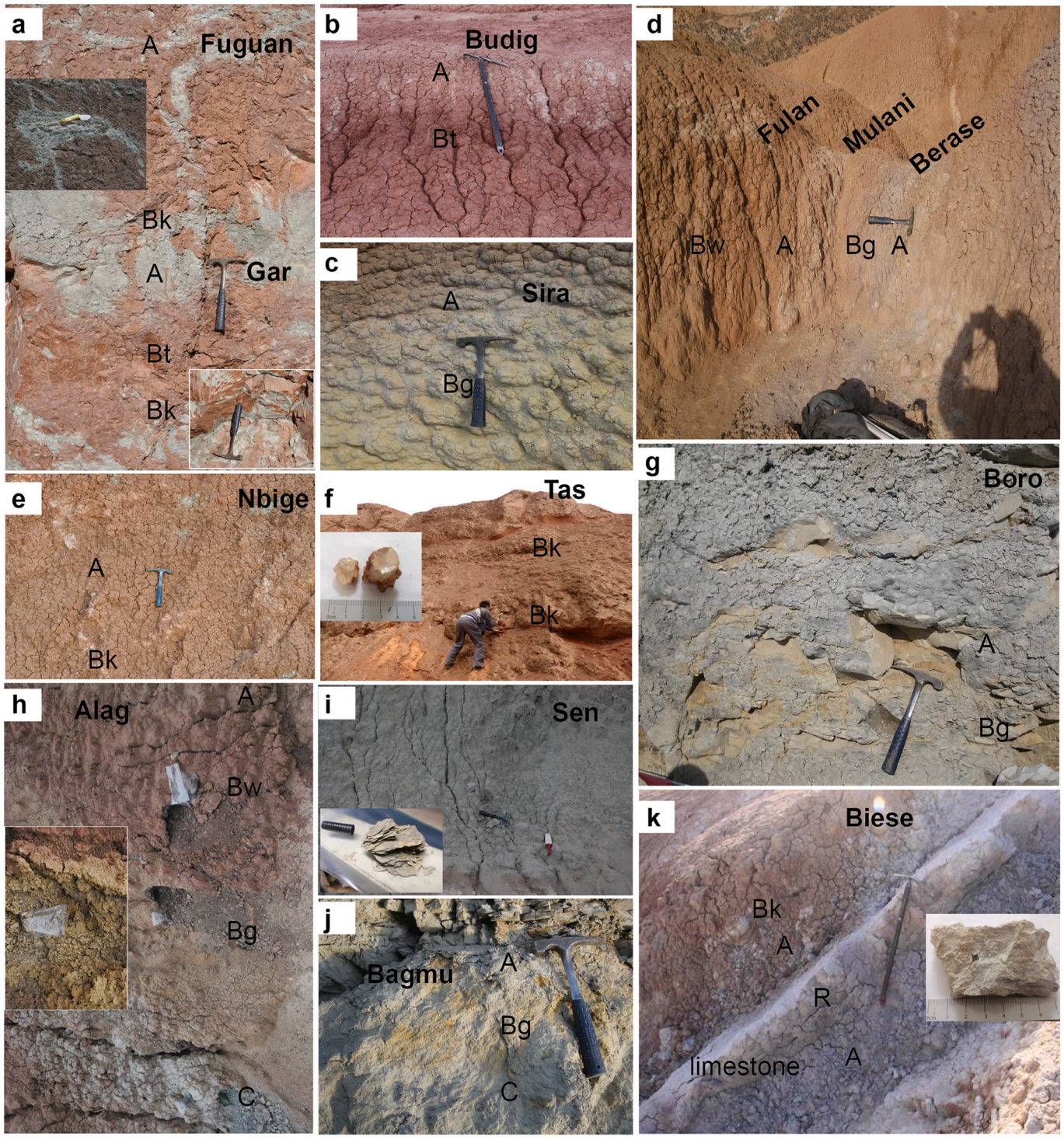

Fig. 2. Paleosol outcrops and soil horizons recognized in Zhangye Danxia. See Fig. 3, Table 1 and text for paleosol naming and pedogenic features.

significance.

2. Geological settings

Zhangye Danxia National Geopark(38°58′28“ N, 100°1’47” E) is located 40 km northwest of Zhangye city, Gansu Province, in the Hexi corridor, northern Qilian Mountains in northwestern China (Fig. 1a). The geological sequence of Zhangye Danxia (Fig. 1b) is the result of extension and rifting of the China north block during the Early Cretaceous, which formed a series of graben basins such as Jiuquan Basin, Zhangye Basin, and Wuwei Basin in adjacent areas (Liu et al., 2017). These basins accumulated alluvial, fluvial and lacustrine sediments (Zheng et al., 2021). The Early Cretaceous stratigraphy in these basins comprises successive Chijinpo Formation, Xiagou Formation, and Zhonggou Formation (Fig. 1e). Postdepositional compression and uplift led to tectonic inversion and erosion, which resulted in Zhangye Danxia's current topography on the flank of a syncline(Fig. 1c, d) and a preserved thickness of 755 m (Fig. 1f) in the Zhangye Danxia section studied here. More details about this section are provided by Liu et al. (2017).

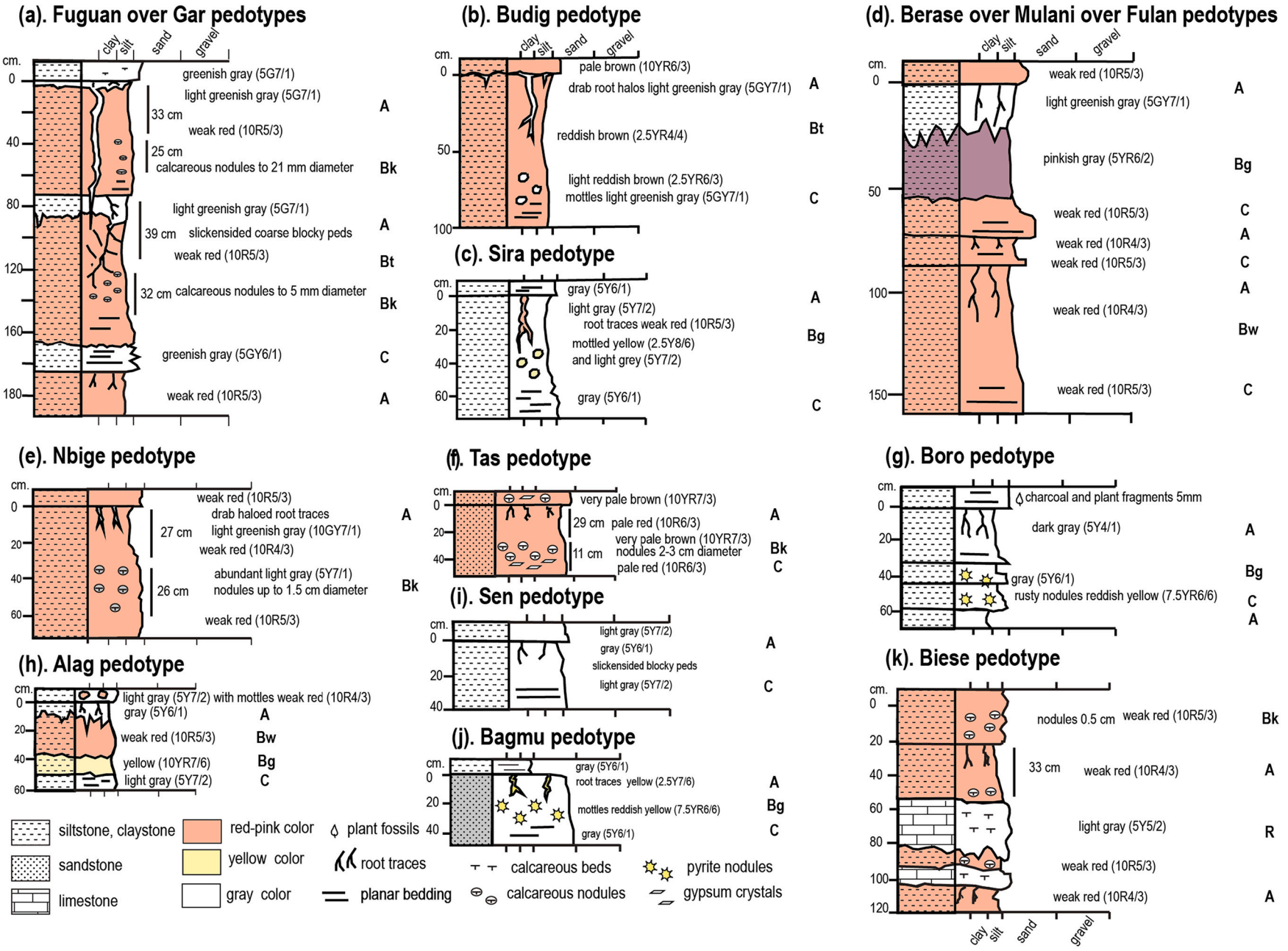

Fig. 3. Pedogenic features and pedotype profiles recognized in Zhangye Danxia section. See text and Table 1 for explanation.

Lithological correlations have suggested that the Zhangye Danxia section includes incomplete Xiagou and Zhonggou Formations (Liu et al., 2013), which are known for fossil plants (Deng et al., 2005; Sun et al., 2013; Yang and Deng, 2007), dinosaurs (Li et al., 2007; You and Li, 2009), and birds (Harris et al., 2006; You et al., 2006) in northwestern China. The Xiagou Formation of non-calcareous red claystones is overlain by Zhonggou Formation of sandstones and conglomerates, with multicolored claystones of red, green yellow and gray (Liu et al., 2013; Zheng et al., 2021).There is controversy over the exact age of the Xiaogou and Zhonggou Formations of the Zhangye Danxia, which are considered Early Cretaceous rocks like the underlying Chijinqiao and Chijinpu Formations (Hao et al., 2000). Ostracods and charophytes from the Xiagou Formation elsewhere in Gansu have been regarded as Barremian in age (Hu and Xu, 2005; Hu, 2004; Wang et al., 2003, 2012), but a pollen assemblage was considered Hauterivian in age (Liu, 2000). Pollen in the Zhonggou Formation is considered early Albian (Zhang et al., 2015). Insects in the Xiagou Formation are similar to the Barremian-Aptian Jehol biota (He et al., 2004; You et al., 2006). Zircon U—Pb dating of basalts in the Xiagou Formation of the Hanxia Section yielded an age span of 115–125 Ma, or Aptian (Li et al., 2013). Also Aptian-Albian were lava flows dated by K—Ar at 106.6 ± 2.2 Ma and 112.0 ± 0.6 Ma from Hongliuxia in the Yumen area, and 112.8 ± 3.4 Ma and 118.8 ± 3.6 Ma from Jianquanzi (Li and Yang, 2004). Cyclostratigraphic analysis of magnetic susceptibility of the Xiagou Formation in the lower part of Zhangye Danxia has been used to suggest an age range of 114.1 Ma to 120.2 Ma (Liu et al., 2017). Carbon isotopic study of lacustrine facies of the Xiagou Formation have suggested correlation with the Selli oceanic anoxic event (Suarez et al., 2013), now dated as early Aptian (125.3 Ma) age (Ogg et al., 2016). Recent biostratigraphical and chronostratigraphical work in Jiuquan Basin suggested late early Aptian-early Albian in age for the Xiagou Formation, with an age of 112.4 ± 0.3 Ma for the base of the Zhonggou Formation (Zheng et al., 2021). In the present study, the age model for Xiagou Formation in Zhangye Danxia section from Liu et al. (2017) is accepted (Fig. 1e), that is a range of 120.2 Ma at the bottom of the local section to 114.1 Ma at level 474 m. Assuming a sediment accumulation rate in Zhonggou Formation similar to that of the Xiagou Formation, yields an estimated age of 110.5 Ma at the (755 m) as illustrated in Fig. 1e.

Zhangye Danxia is well known for its brilliant multicolored landscapes (Fig. 1g) with alternating colors of red, yellow, and gray characteristic of various paleosols (Fig. 2), similar to the Painted Hills of Oregon, USA (Retallack et al., 2000). The Zhangye Danxia section is dominated by mudstone and siltstone with few occurrences of sandstone and conglomerate (Fig. 1d, f). Liu et al. (2017) divided Zhangye Danxia section into six subsections based on color, lithology, and sediment rhythmicity, inferring a variety of paleoclimatic and paleoenvironmental stages.

3. Materials and methods

Zhangye Danxia section is perfectly exposed with little cover by plants or sediments of other geological ages (Fig. 1g landscape photos), so that paleosol profiles crop out, and can be further exposed by trenching (Fig. 2). Individual pedotypes were repeated in the section, and each pedotype was described, classified, sampled, measured, and subject to detailed examination as it was encountered in the section. Thus, it was not necessary, and also forbidden by the geopark, to trench the entire section.

Paleosols were recognized and classified in the field based on root traces, soil horizons, and soil structures. Root traces are the direct evidence that the rock or sediment was colonized by plants (Retallack, 1988). Root traces are well preserved in waterlogged paleosols, which allows preservation of original organic matter. In red paleosols, root traces, usually in form of drab-haloes, can be recognized according to their features of downward branching and tapering, irregular and tubular shape. Gradual transition between soil horizons is another striking feature distinct from sedimentary bedding whose boundaries are mostly sharp. A paleosol profile observed in the field usually has a sharp surface, above root traces and other soil horizon transitions. Original paleosol profiles may be partly eroded by subsequent fluvial or alluvial sediment (Tabor and Myers, 2015), in particular A horizon and O horizons. Soil structures have the overall effect of homogenizing and destroying original sedimentary bedding, so that the claystones appear massive, hackly and jointed.

The Zhangye Danxia pedotypes were named using the Monguor local language (De Smedt and Mostaert, 1964), as a non-genetic terminology for particular kinds of paleosols (Retallack, 1994). Each paleosol was assessed for degree of development from profile form, for carbonate content using dilute acid, and for hue (5Y to 5R) using a Munsell color chart (Retallack, 1997). Both development and carbonate content scales had five levels: very weak, weak, moderate, strong, and very strong, pegged to destruction of bedding or nodular carbonate for moderate development, and clear effervescence in dilute (0.1 mol) HCl for moderate calcareousness (Retallack, 1988).

Paleosols in Zhangye Danxia are here classified within modern soil taxonomy of Food and Agriculture Organization (FAO). The Food and Agriculture Organization classification is especially useful for interpreting paleosols because it is linked to soil maps of the world. Paleosol classifications can be used to guide the search for modern analogues that reveal conditions of formation in the past. This method of interpreting paleosols supplements the classical factor-function approach to paleosol interpretation (Retallack, 2019).

Undisturbed bulk samples ($n = 21$) were collected and cut to make thin sections following procedures of Tate and Retallack (1995) with kerosene to avoid clay expansion. Soil micromorphology was determined and described under microscope with plan and cross polarized light.

For calcic paleosols with Bk horizon, the mean annual precipitation (MAP) is estimated by the depth from soil surface to the Bk horizon following.

$$\text{MAP (mm yr}^{-1}) = -0.013D^2 + 6.45D + 137.2$$

where D is Bk depth (cm) to paleosol top, SE is ±147 mm yr^{-1}, and R^2 is 0.52. Note that D is the decompaction depth corrected according to Sheldon and Retallack (2001).

Selected samples ($n = 44$) of each paleosol profile were imparted by diffuse reflectance spectroscopy (DRS) using a UV-2600 spectrophotometer (Shimadzu Instruments Manufacturing Co., Ltd.) with a wavelength range of 400–700 nm in 1 nm increment. The peaks at ~435/535 nm and 575 nm of DRS spectral patterns are widely interpreted as proxies for goethite and hematite content, respectively (Deaton and Balsam, 1991; Ji et al., 2002). Because the peak of goethite at 535 nm is suppressed by hematite, the peak at 435 nm is regarded as goethite instead. The ratio of peaks at ~575 nm and ~ 435 nm is used as the ratio of hematite and goethite (Hm / Gt). Because hematite is the end product of iron oxides in a dry oxidizing environment, and goethite commonly appears in a waterlogged oxidizing environment (Hu et al., 2013; Schwertmann, 1988), the ratio Hm / Gt deduced from DRS is thus inversely proportional to degree of waterlogging (Ji et al., 2002; Lepre and Olsen, 2021). In the present study, the Hm / Gt of an individual pedotype is defined as the average of B horizons, or A and C horizons if B horizon does not exist in such pedotype.

4. Results and discussion

4.1. Paleosol identification, classification and description

Paleosol outcrops found in the Zhangye Danxia section are shown in Fig. 2, and sketched in Fig. 3. Drab-haloed root traces are very common in red paleosols (Fig. 2a, b), while root traces in gray paleosols are reddish or yellow (Fig. 2j). Most paleosols in Zhangye section were preserved with root traces indicative of an A horizon (Fig. 3). There are various B horizons in Zhangye Danxia including clayey Bt horizons with

Table. 1
Pedotypes, diagnosis and classification for Zhangye Danxia paleosols.

Pedotype	Orthography	Monguor	Level in section	Diagnosis	FAO classification and code
Alag	alaĢ	Multicolored	658 m	Gray silty surface (A) over purple silty surface (Bw), over yellow siltstone (Bg)	Eutric Gleysol (Ge)
Bagmu	baÇmu	Separate	558 m	Gray sandstone (A) over yellow and orange sandy subsurface (Bg)	Gleyic Solonchaks (Zg)
Berase	bẹrāsẹ	Wine	210 m	Gray silty surface (A) grading down to purple subsurface (Bg)	Eutric Gleysol (Ge)
Biese	biesẹ	Resistant	396 m	Red silty surface (A) with drab-haloed root traces over thick calcareous bench (K)	Calcaric Gleysol (Gc)
Boro	Boro	Gray	646 m	Dark gray silty surface (A) over orange rusty goethite nodules in gray siltstone (Bg)	Humic Gleysol (Gh)
Budig	Budȉg	Dye	255 m	Silty surface with drab-haloed root traces (A) over gradual transition of clayey slickensided subsurface (Bt)	Orthic Luvisol (Lo)
Fuguan	fuGuän	Deep	275 m	Silty surface with drab-haloed root traces (A) over calcareous nodules (Bk) at >30 cm depth	Calcic Xerosol (Xk)
Fulan	fulān	Red	210 m	Red clayey surface (A) over blocky subsurface (Bw) and orange subsurface (C)	Eutric Cambisol (Be)
Gar	Ģar	Fire	275 m	Silty surface with drab-haloed root traces (A) over slickensided clay (Bt) and deep calcareous nodules (Bk)	Calcic Luvisol (Lk)
Mulani	mulāni	Small	210 m	Red clayey surface (A) on bedded red subsurface (C)	Eutric Fluvisol (Je)
Nbige	nbìGe	Egg	306 m	Red silty surface with drab haloed root traces (A) over large calcareous nodules (Bk) at <30 cm	Calcic Xerosol (Xk)
Sen	sẹn	Layer	566 m	Dark gray claystone (A) over bedded shale (C)	Eutric Fluvisol (Je)
Sira	śira	Yellow	250 m	Gray silty surface with red cracks down to subsurface (Bg) with jarosite after pyrite	Humic Gleysol (Gh)
Tas	t'aṣ	Rock	755 m	Red sandy surface (A) over large calcareous nodules (Bk) and gypsum crystals	Calcic Yermosol (Yk)

slickensides (Figs. 2a, 3a), calcareous nodular subsurface (Bk) horizons (Figs. 2e, 3e), and colored/structural subsurface (Bw) horizons (Figs. 2h, 3h). C horizons in a paleosol profile usually have sedimentary relicts such as bedding, but a C horizon may be missing in successive paleosols that overlap lower paleosols in the stack (Fig. 3a). Soil structure in Zhangye Danxia section includes blocky peds defined by clay skins that are slickensided (Figs. 2a, 3a). Calcareous nodules are also soil structures comparable with modern caliche (Fig. 2a, e, f, k).

Based on the criteria above and their repeated occurrence in the section, a total of 155 paleosol profiles of 14 different pedotypes were recognized (Fig. 2, Fig. 3), with 95 paleosol profiles in the Xiagou Formation (0–474 m) and 60 paleosol profiles in the Zhonggou Formation (474–755 m). Each pedotype, named using the Monguor local language for specific meaning, was distinguished based on their pedogenic features visible in the field, and classified within modern soil taxonomy of Food and Agriculture Organization (FAO) based on diagnostic features. The following notes outline each pedotype at well exposed examples considered type profiles, and its classification within the Food and Agriculture Organization (1978, 1977), also summarized in Table 1.

(1) Pedotype Fuguan at 275 m means “deep” in Monguor language due to the deep Bk horizon (Fig. 2a, Fig. 3a). It has silty surface with drab-haloed root traces (A) over calcareous nodules (Bk) at >30 cm depth (Fig. 2a, insert top). Slickensided peds are obvious in the A horizon, and the diameter of calcareous nodules within the Bk horizon is up to 5 mm. The pedotype Fuguan has deep calcareous nodules, and a gray surface horizon indicative of the relatively high plant productivity of a Calcic Xerosol (FAO map code Xk).

(2) Pedotype Gar at 275 m is named for “fire” in Monguor language, because of its dark red color (Fig. 2a, Fig. 3a). It has a silty surface with drab-haloed root traces (A) over slickensided (Fig. 2a, insert bottom) clay (Bt) and deep calcareous nodules (Bk). Clay-rich subsurface (Bt) horizons of pedotype Gar are comparable with Luvisols of FAO classification, while the additional deep horizon of calcareous nodules defines it as Calcic Luvisol (map code Lk).

(3) Pedotype Budig at 255 m means “dye” in Monguor language (Fig. 2b, Fig. 3b). It has a silty surface with drab-haloed root traces (A) over gradual transition to clayey slickensided subsurface (Bt). Its clay-rich Bt horizon, and lack of Bk horizon is like Orthic Luvisol (map code Lo) within FAO classification.

(4) Pedotype Sira at 250 m, meaning “yellow” in Monguor language (Fig. 2c, Fig. 3c), is named for yellow mottles. It shows gray silty surface with red cracks down to a subsurface horizon (Bg) with jarosite mottles after pyrite. The smectite clays and pyrite are evidence of waterlogging, and allow identification as Humic Gleysol (map code Gh). The Sira pedotype reoccurs in cyclic alternation of pedotypes between depth 50–250 m (Fig. 2g), as evidence of waterlogged culminations of climate cycles.

(5) Pedotype Berase at 210 m, meaning “wine” in Monguor language, is named for its purple subsurface (Fig. 2d, Fig. 3d). It has gray silty surface (A) grading down to thin purple subsurface (Bg). The gray surface and gleyed subsurface are like Eutric Gleysol (map code Ge).

(6) Pedotype Mulani at 210 m, meaning “small” in Monguor language, is named for modest thickness (<20 cm) (Fig. 2d, Fig. 3d). It has red clayey surface (A) on bedded red subsurface (C) in absence of B horizon, indicating very weak development, like an Eutric Fluvisol (map code Je).

(7) Pedotype Fulan at 210 m, meaning “red” in Monguor language, is named for the weak red color (<20 cm) (Fig. 2d, Fig. 3d). It shows red clayey surface (A) over blocky subsurface (Bw) and orange subsurface (C). It resembles Eutric Cambisol (map code Be), because its subsurface horizon is insufficiently clayey to qualify as argillic.

(8) Pedotype Nbige at 306 m, meaning “egg” in Monguor language, is named for the occurrence of large calcareous nodules (up to 5 cm diameter) (Fig. 2e, Fig. 3e). It has a red silty surface with drab haloed root traces (A) over large calcareous nodules (Bk) at <30 cm, like Calcic Xerosol (map code Xk).

(9) Pedotype Tas at 755 m, meaning “rock” in Monguor language, looks like rock due to common gypsum crystals (Fig. 2f, Fig. 3f). It has red sandy surface (A) over large calcareous nodules (Bk) and gypsum crystals (By) (Fig. 2f, insert), which is similar to Calcic Yermosol (map code Yk) with coexistence of calcareous nodules and gypsum crystals.

(10) Pedotype Boro at 646 m, is named for its color and means “gray” in Monguor language (Fig. 2g, Fig. 3g). It has dark gray silty surface (A) over orange rusty goethite nodules in gray siltstone (Bg). High chroma mottles are characteristic of waterlogging (Vepraskas and Richardson, 2000) found in Gleysols, and its dark surface is like a Humic Gleysol (map code Gh).

(11) Pedotype Alag at 658 m is named for its color meaning “multicolored” in Monguor language (Fig. 2h, Fig. 3h). It shows gray silty surface (A) over purple silty surface (Bw), over yellow siltstone (Bg) (Fig. 2h, insert). The smectite clays of the Alag pedotype and its gleyed subsurface are like Eutric Gleysols (map code Ge).

(12) Pedotype Sen at 566 m, meaning “layer” in Monguor language, refers to sedimentary bedding (Fig. 2i, Fig. 3i). It is weakly

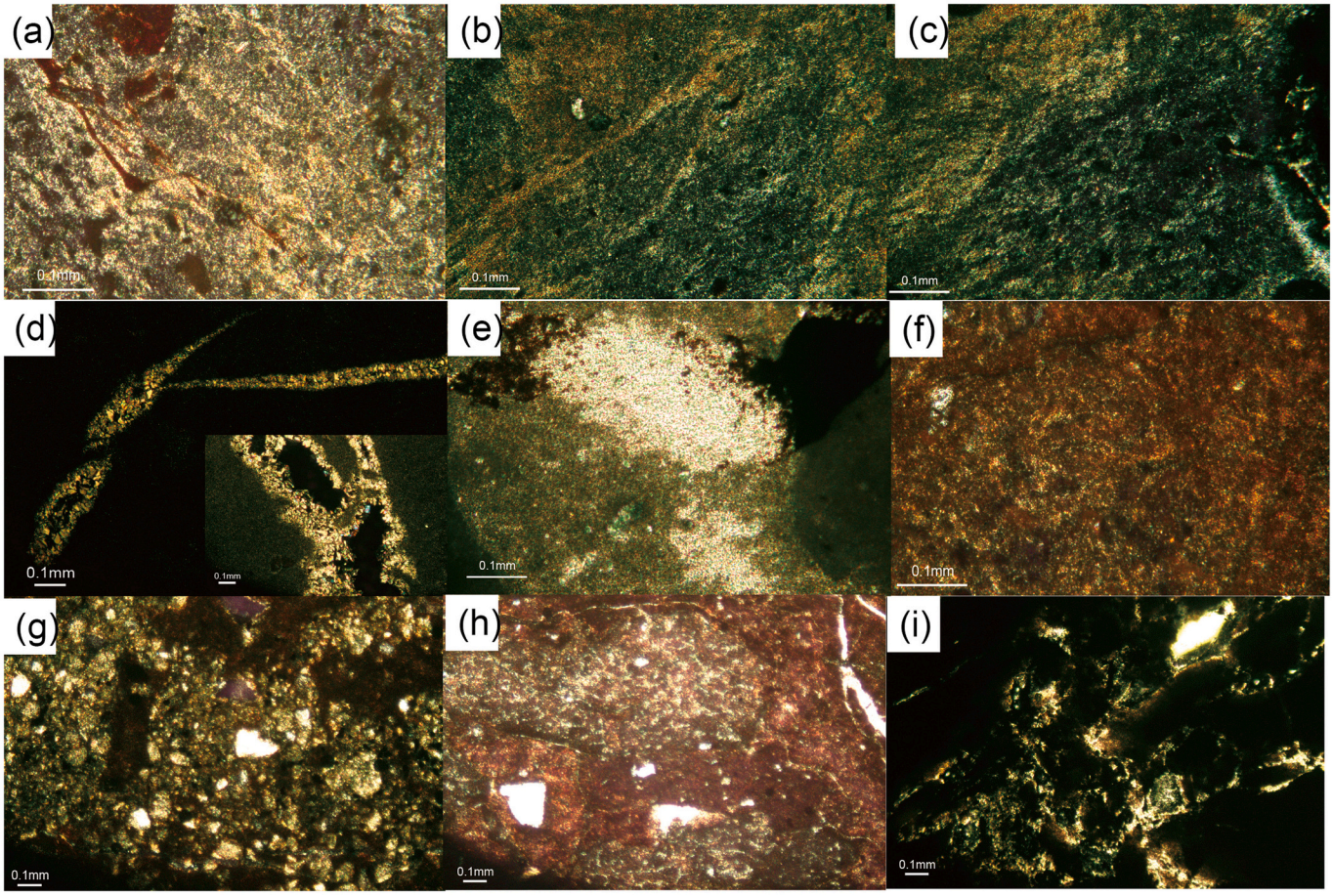

Fig. 4. Micromorphology of Zhangye Danxia paleosols. All images are in cross polarized light. The scale is 0.1 mm. (a) F108 (Fuguan), clinobimasepic porphyroskelic fabric with some pedorelicts (papules). (b) F108 (Fuguan), bimasepic fabric. (c) D339 (Sira), climobimasepic plasmic fabric. (d) Q194 (Alag), mycorrhizal chambering of a root trace with fungal needle-fiber calcite. (e) ZYR3 (Sira), micritic displacive pedogenic nodule (calciasepic porphyroskelic) with iron-manganese mottles to the left. (f) B100 (Fulan), bimasepic porphyroskelic. (g) B100 (Fulan), agglomeroplasmic calciasepic. (h) ZYR4 (Berase), argillans (laminated around clasts). The clasts appear to be calciasepic nodules. (i) D339 (Sira), amorphous iron-manganese staining off cracks in a micrite, indicating gleization.

developed and has dark gray claystone (A) with carbonaceous root traces over bedded shale (Fig. 2i, insert) (C). Pedotype Sen is thin, smectitic, with relict bedding, similar to Eutric Fluvisols (map code Je) in FAO system.

(13) Pedotype Bagmu at 558 m, meaning “separate” in Monguor language, is clearly different from the overlying bedding (Fig. 2j, Fig. 3j). It has gray sandstone (A) over yellow and orange sandy subsurface (Bg). Bagmu paleosols have much relict bedding, indicating weak development, as well as an unusual sandy texture and yellow mottles, like Gleyic Solonchaks (map code Zg) in FAO system.

(14) Pedotype Biese at 396 m, meaning “resistant” in Monguor language, includes a thick tabular limestone (Fig. 2k, Fig. 3k). It has red silty surface (A) with drab-haloed root traces over thick calcareous bench (K) (Fig. 2k, insert). The Biese pedotype has some micrite and nodularization, but also ostracods and charophytes as evidence that the limestone is lacustrine, and thus a calcareous parent material rather than a pedogenic petrocalcic horizon. Biese paleosols are thus regarded as weakly developed paleosols from eutrophication of calcareous ponds, or Calcaric Gleysols (map code Ge).

Comparison of groups of paleosols in the uppermost Zhangye Danxia section with map units of FAO found analogues among the Xerosols and Yermosols in China, but other combinations of paleosols compared better with map units in South Asia than China (Food and Agriculture Organization, 1978, 1977), which suggests more humid and warmer paleoclimate than at present.

4.2. Soil micromorphology

Petrographic thin sections have been widely used to investigate soil micromorphology (Brewer, 1976). Different soil micromorphologies can be distinguished from the proportion and distribution of plasma (clay and iron stains), skeleton grains (e.g., quartz, feldspar) and open space (e.g., voids). Sepic plasmic fabrics, with streaks of highly birefringent and highly oriented clay, are diagnostic of soil and paleosols with few exceptions. Zhangye Danxia thin sections demonstrate various sepic plasmic fabrics as evidence of paleosols in Fig. 4, e.g., clinobimasepic porphyroskelic fabric (Fig. 4a, c), bimasepic fabric (Fig. 4b, f), and agglomeroplasmic calciasepic (Fig. 4g). In addition, some other pedogenic features include root traces (Fig. 4d), calcite nodules (Fig. 4e), argillans and gleization (Fig. 4h).

4.3. DRS for characterizing hematite and goethite

The formation and transformation of iron oxides in soils and paleosols are sensitive to the degree of waterlogging(Schwertmann, 1988), as indicated by different colors ranging from red to yellow and gray. Hematite is responsible for the red color in soils, and is formed and stabilized in well-drained oxidizing conditions, but yellow-brown colors due to goethite in soils are an indication of waterlogging. In spite of the fact

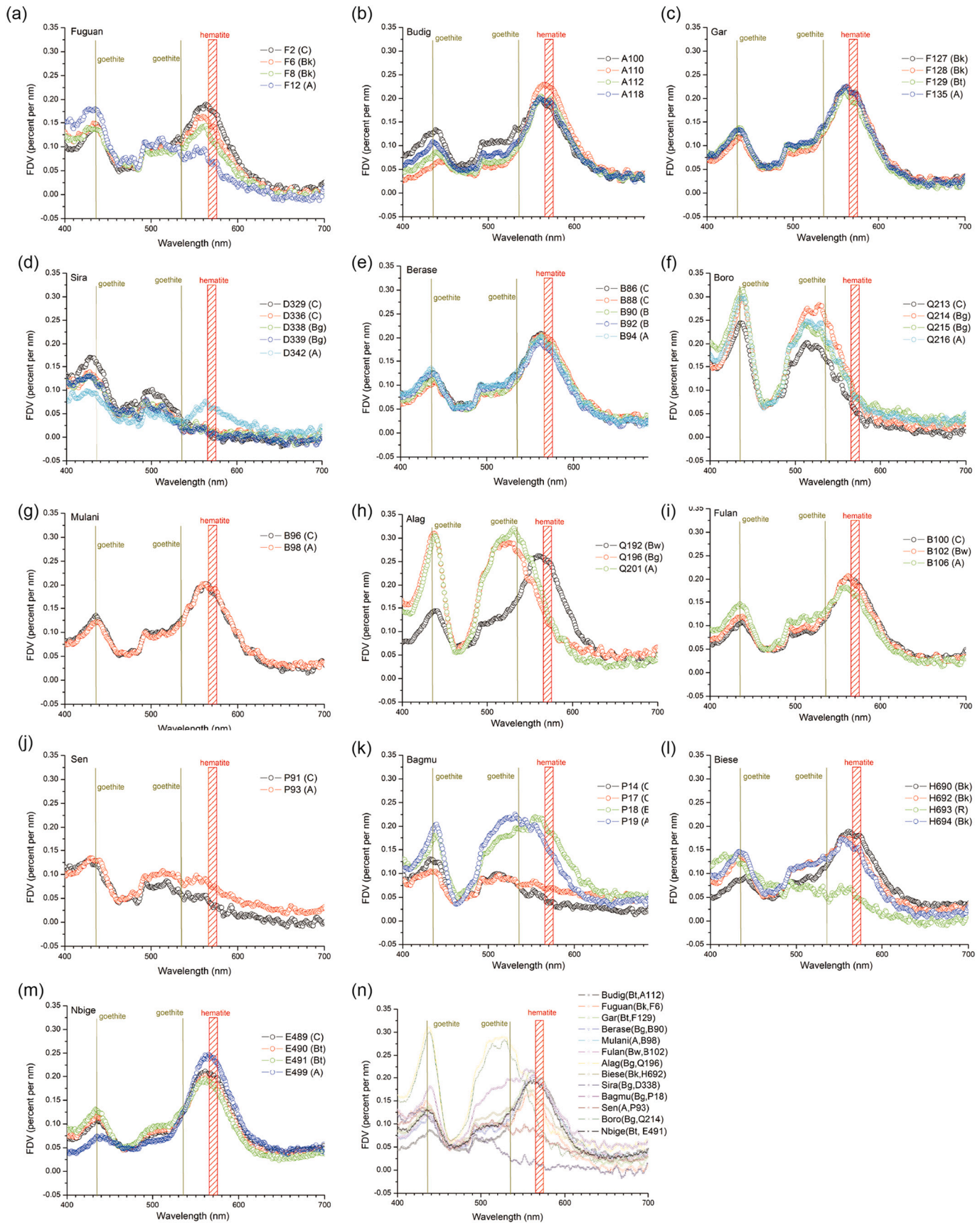

Fig. 5. First-order derivative variations (FDV) of diffuse reflection spectra (DRS) of Zhangye Danxia pedotypes. (a-m) FDV of individual pedotypes. (n) a comparison of each pedotype. Peak at 565–575 nm (red rectangle) is diagnostic of hematite. Peaks at 435 nm and 535 nm (dark yellow lines) are diagnostic of goethite. DRS measurements of pedotype Tas is not available. (For interpretation of the references to color in this figure legend, the reader is referred to the web version of this article.)

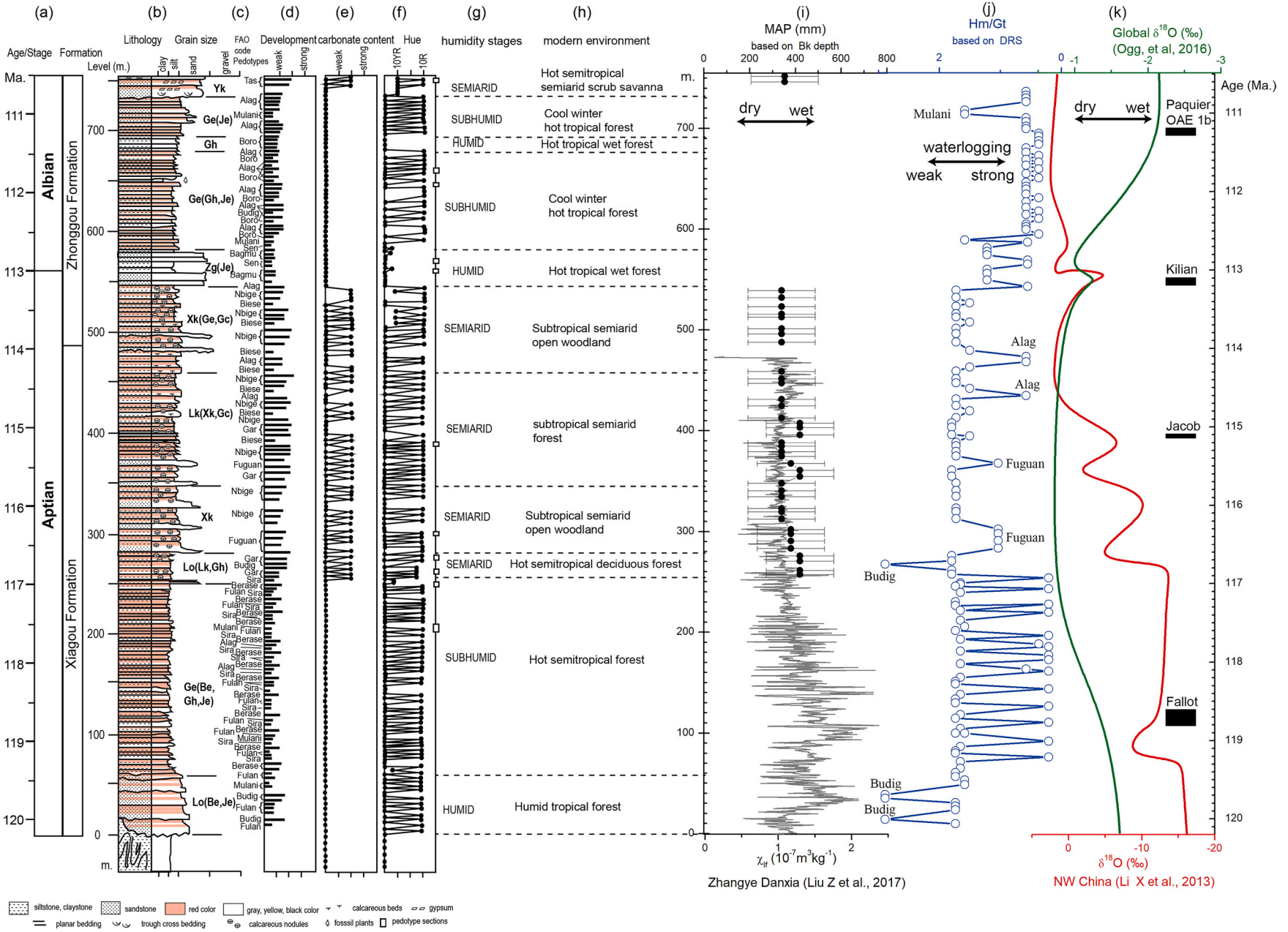

Fig. 6. Paleosol succession characterization, soil units and environment in Zhangye Danxia section. (a) age is from Liu et al. (2017). (b) lithological stratigraphy of Zhangye Danxia section mapped in the field. (c) FAO pedotype code and soil unit, see Table 2 for details. (d) paleosol development boxes are based on the soil maturity scale (Retallack, 2019). (e) carbonate content as a proxy of aridity is based on field reaction with dilute HCl (Retallack, 2019). (f) Munsell hue as a proxy of waterlogging or drainage. (g) humidity stages derived from FAO soil units. (h) modern environment of FAO soil units in south Asia. (i) reconstructed MAP based on Bk depth. (j) ratio of Hematite (Hm) and goethite (Gt) based on DRS measurements. (k) carbonate oxygen isotope in NW China (Li et al., 2013) and global oxygen isotope records with oceanic anoxic events (OAE) during Aptian and Albian (Ogg et al., 2016).

that quantitative relationship and transformation between goethite and hematite could be influenced by many factors (Schwertmann, 1988) such as soil temperature, soil humidity, pH, organic matter, burial reddening and Al substitution (Liu et al., 2011), the concentration of hematite or the ratio of hematite/goethite (Hm / Gt) has been used to be a proxy for aridity or humidity (Lepre and Olsen, 2021). DRS measurements have been widely used to quantify hematite and goethite in loess-paleosol and red bed sediments (Ji et al., 2002; Lepre and Olsen, 2021). The amplitude and position of the characteristic absorption peak of hematite (~565–575 nm) and goethite (~435 nm or ~ 535 nm) increase with their concentrations.

The first-order derivative variation (FDV) of Zhangye Danxia pedotypes are shown in Fig. 5, which visually demonstrates differences in waterlogging (reducing/oxidizing) of each pedotype. Firstly, red pedotypes, such as Fuguan (Fig. 5a), Budig (Fig. 5b), Gar (Fig. 5c), Berase (Fig. 5e), Mulani (Fig. 5g), Fulan (Fig. 5i), Nbige (Fig. 5m), are dominated by hematite with less goethite due to good drainage. Secondly, burial gleization in the form of drab-haloed root traces reduces the hematite peak in A and B horizons of Fuguan (Fig. 5a), and Budig pedotypes (Fig. 5b). Thirdly, gray pedotypes with yellow mottles, sucha as Boro (Fig. 5f) and Bagmu (Fig. 5k), or horizon such as Alag (Fig. 5h) have goethite peaks at 435 nm and 535 nm, but no hematite peak at 565–575 nm, indicating seasonally waterlogged environment. Finally, increasing gleization results in completely gray paleosols or horizons, as in the pedotypes Sira (Fig. 5d), and Sen (Fig. 5j), and the C horizon of Bagmu (Fig. 5k), and R layer of Biese (Fig. 5l). These gray rocks have no hematite and very little goethite, indicating a reducing environment. Different degrees of waterlogging in paleosols leads to a decrease of hematite but increase of goethite, whereas deep gleization leads to a complete dissolution of iron oxides (Hu et al., 2015). Therefore, the DRS results of Zhangye paleosols, that is the amplitude of characteristic peaks of hematite and goethite, indicate relative waterlogging in paleosols.

4.4. Palaeoclimatic implication deduced from paleosol successions

Systematic work of paleosol identification and classification based on pedogenic features in the field allows characterization of the paleosol succession in the 755-m-thick section (Fig. 6c), together with notes on their development (Fig. 6d), carbonate content (Fig. 6e) and hue (Fig. 6f). Soil color is an indication of redox conditions inferred from particular oxygen-sensitive minerals (Scheinost and Schwertmann, 1999). Red soil color is from hematite, brown from goethite, yellow from jarosite or goethite, and gray from organic matter with reduced (ferrous) iron (Retallack and Dilcher, 2012; Retallack and Kirby, 2007). Red paleosols indicate low water tables, gray paleosols indicate high water tables, and yellow paleosols may be of salinas, salt marsh, or mangal (Retallack, 2013). The frequent alternation of paleosol color in Zhangye Danxia section (Fig. 3f) indicates variations in both precipitation and waterlogging.

The relative degree of paleosol development is estimated based on soil maturity indicated by development of soil horizons and pedogenic features (Retallack, 2019), the thicker soil horizons the stronger development, suggesting longer time for paleosol formation (Retallack, 1984), though other factors such as topography and climate possibly increase or decrease the duration. Pedotypes Fuguan, Gar, Nbige, Tas and Budig with thicker Bt and Bk horizons show stronger development than other pedotypes. In Zhangye Danxia section between levels 250 m and 546 m, most paleosols are moderately developed, whereas paleosols of weak development dominate below and above these levels (Fig. 6d). Because soil carbonate is widespread in dryland soils, but is leached entirely in humid climates, soil carbonate content is related to precipitation (Retallack, 2005; Tabor and Myers, 2015). Based on the correlation between the depth to Bk horizon and mean annual precipitation (MAP) (Retallack, 2005) in dryland paleosols, the pedotypes with measured Bk depth such as Fuguan (Fig. 3a), Gar (Fig. 3a), Nbige (Fig. 3e), Tas (Fig. 3f) give MAP 380 mm, 420 mm, 339 mm, 353 mm, respectively, indicating semiarid environments at the level 250–546 m and 740–745 m (Fig. 6i). Note that the MAP of pedotype Tas might be underestimated because the occurrence of gypsum crystals indicates much lower MAP (Retallack and Huang, 2010). Despite semimarid to arid climate there were local oases of high water table in the floodplain, as indicated by gleyed paleosols, FAO code Ge, Gh, Gc. Paleosol development and carbonate content roughly divides the section in four stages. (1) At level 0–255 m (lower Xiagou Formation, early Aptian), most paleosols show weak development and low carbonate content, indicating shorter time for soil formation and humid-subhumid environments. Impressively, 12 similar cycles of Sira, Fulan, and Berase pedotypes are repeated between 50 and 250 m (Fig. 1g), suggesting periodic changes of paleoclimate (Liu et al., 2017). (2) At level 250–546 m (upper Xiagou Formation, late Aptian), Calcic paleosols of moderate development dominate, thus indicating relatively longer time for soil formation and semiarid paleoclimate. (3) At level 546–740 m (lower Zhonggou Formation, early Albian), gray sandy paleosols (e.g., Sen and Bagmu pedotypes) between 546 and 582 m and colorful paleosols (e.g., Alag) between 582 and 740 m are weakly developed and have low carbonate content, which suggests shorter time for soil formation in humid-subhumid and locally waterlogged environments. (4) At level 740–755 m (Zhonggou Formation, Albian), pedotype Tas (FAO code Yk) is moderately developed with gypsum crystals, indicating a semiarid-arid environment.

More details of paleoenvironmental changes can be deduced by a systematic analysis of paleosol units. The FAO classification is used for interpreting units of paleosols as ancient soilscapes (Retallack, 2019), in which map units are numbered and tabulated (Food and Agriculture Organization, 1977). For example, map unit Lo 50-2a (Be, Lc, G) near

Table 2
Humidity stages of Zhangye Danxia derived from comparing paleosol units to their modern analogues in south Asia.

Interval (m)	FAO code	Most similar FAO soil map unit	Modern environment	Humidity stages from soil units
740–755	Yk	Yk40–2/3a (Zo) around Badin, Pakistan	Hot semitropical semiarid scrub savanna	Semiarid
697–740	Ge (Je)	Ge51-2a (Je,Jc,Be, Gh) in Sirajgang, Bangladesh and nearby India	Cool winter hot tropical forest	Subhumid
680–697	Gh	Gh16–2/3a (Ge,We, Je) in Myinmu, Myanmar	Hot tropical wet forest	Humid
582–680	Ge (Gh, Je)	Ge51-2a (Je,Jc,Be, Gh) in Sirajgang, Bangladesh and nearby India	Cool winter hot tropical forest	Subhumid
546–582	Zg (Je)	Zg4-3a (Je, Jt) Dedaye, Myanmar	Hot tropical wet forest	Humid
460–546	Xk (Ge, Gc)	Xk32-3a (Gc, Rc) in Shiraz, Iran	Subtropical semiarid open woodland	Semiarid
348–460	Lk (Xk, Gc)	Lk5-3ab (I,Lc,E,Rc,Z) east of Amman, Jordan	subtropical semiarid forest	Semiarid
282–348	Xk	Xk32-3a (Gc, Rc) in Shiraz Iran	Subtropical semiarid open woodland	Semiarid
250–282	Lo (Lk, Gh)	Lo49-2a (Be, Lk) at Gaya, India	Hot semitropical deciduous forest	Semiarid
55–250	Ge (Be, Gh, Je)	Ge12–1/2a (Be) in Rangpur Bangladesh and nearby India	Hot semitropical forest	Subhumid
0–55	Lo (Be, Je)	Lo 50-2a (Be, Lc, G) near Durgapur, India	Humid tropical forest	Humid

Table 3
DRS data of each pedotype for characterizing hematite (Hm) and goethite (Gt). The Gt wavelength is at ~435 nm and Hm wavelength is at ~565 nm.

Pedotype	Sample (horizon)	Gt wavelength (nm)	Gt Peak value (1st order)	Hm wavelength (nm)	Hm Peak value (1st order	Hm / Gt
Fuguan	F2 (C)	438	0.1455	563	0.1899	1.3058
	F6 (Bk)	434	0.1494	559	0.1647	1.1023
	F8 (Bk)	435	0.1483	563	0.1443	0.9728
	F12 (A)	435	0.1807	–	–	–
Budig	A100 (C)	438	0.1333	561	0.2022	1.5174
	A110 (Bt)	442	0.0672	565	0.2299	3.4198
	A112 (Bt)	438	0.0866	561	0.2052	2.3687
	A118 (A)	435	0.1087	559	0.2016	1.8549
Gar	F127 (Bk)	438	0.1183	562	0.2237	1.8906
	F128 (Bk)	436	0.1169	562	0.2250	1.9248
	F129 (Bt)	437	0.1377	561	0.2173	1.5787
	F135 (A)	437	0.1339	563	0.2264	1.6904
Sira	D329 (C)	427	0.1714	–	–	–
	D336 (C)	427	0.1384	–	–	–
	D338 (Bg)	426	0.1324	552	0.0331	0.2498
	D339 (Bg)	428	0.1316	562	0.0213	0.1621
	D342 (A)	423	0.0983	563	0.0766	0.7795
Berase	B86 (C)	437	0.1259	562	0.2093	1.6623
	B88 (C)	439	0.1058	563	0.2070	1.9574
	B90 (Bg)	438	0.1174	563	0.2050	1.7459
	B92 (Bg)	435	0.1236	560	0.1929	1.5604
	B94 (A)	436	0.1352	562	0.2030	1.5021
Boro	Q213(C)	436	0.2446	–	–	–
	Q214 (Bg)	438	0.3004	565	0.1192	0.3969
	Q215 (Bg)	438	0.3154	565	0.1083	0.3435
	Q216 (A)	438	0.3004	–	–	–
Mulani	B96 (C)	436	0.1352	562	0.2030	1.5021
	B98 (A)	436	0.1216	562	0.2027	1.6663
Alag	Q192 (Bw)	438	0.1441	559	0.2626	1.8226
	Q196 (Bg)	437	0.3104	–	–	–
	Q201 (A)	438	0.3050	–	–	–
Fulan	B100 (C)	438	0.1072	562	0.2034	1.8974
	B102 (Bw)	438	0.1196	562	0.2078	1.7378
	B106 (A)	435	0.1461	561	0.1830	1.2528
Sen	P91(C)	426	0.1295	565	0.0485	0.3743
	P93 (A)	430	0.1343	552	0.0981	0.7308
Bagmu	P14 (C)	431	0.1304	565	0.0495	0.3798
	P17 (C)	432	0.1052	552	0.0843	0.8019
	P18 (Bg)	439	0.1810	554	0.2201	1.2164
	P19 (A)	439	0.2042	531	0.2256	1.1047
Biese	H690 (Bk)	442	0.0935	561	0.1893	2.0251
	H692 (Bk)	434	0.1354	554	0.1748	1.2916
	H694 (Bk)	433	0.1457	552	0.1728	1.1864
	H693 (R)	435	0.1207	552	0.0745	0.6168
Nbige	E489 (Bk)	434	0.1083	562	0.2117	1.9544
	E490 (Bk)	434	0.1164	562	0.2021	1.7363
	E491 (Bk)	434	0.1309	562	0.1945	1.4858
	E499 (A)	442	0.0749	566	0.2473	3.3003

Durgapur, India, is mainly Orthic Luvisols (Lo), with inclusions and associated Eutric Cambisols (Be), Chromic Luvisols (Lo) and Gleysols (Food and Agriculture Organization, 1977). This particular soil association concept can be compared with a succession of paleosols including a diversity of pedotypes, with the most common or best developed paleosols used to characterize the interpreted paleosol map unit, such as Lo (Be, Je) from 0 to 55 m in the Zhangye Danxia section (Fig. 6c). Based on comparisons to their analogues in modern environments, the humidity states, temperature and vegetation characteristic of one soil unit can be estimated. Accordingly, the paleoenvironments of Zhangye Danxia section can be described in eleven stages illustrated in Fig. 6g, h and Table 2. For example, at level 460–546 m, pedotype Nbige (Xk) dominates with occurrence of pedotypes Alag (Ge) and Biese (Gc), suggesting soil unit of Xk (Ge, Gc). The paleosol unit Xk (Ge, Gc) is most similar with FAO soil map unit Xk32-3a (Gc, Rc) found in Shiraz, Iran, where is characteristic of subtropical semiarid open woodland (Table 2) (Food and Agriculture Organization, 1978, 1977). The paleoenvironments estimated in this way provide a qualitative change of humidity at cost of ignoration of some detailed variation, for example the occurrence of Gleysol Alag, indicating a humid environment, within the semiarid stages at level 348–546 m.

4.5. Waterlogging variation deduced from DRS

In Zhangye Danxia section, the paleosol units reveal alternation of soil drainage, but more detailed waterlogging variation can be inferred from the relative concentration of goethite and hematite deduced from DRS. The peak values at ~435 nm for goethite (Gt) and ~ 565 nm for hematite (Hm) and the ratio of Hm / Gt based on DRS measurements are summarized in Table 3 and plotted in Fig. 6j. Generally, the value of Hm / Gt is inversely proportional to waterlogging conditions with one exception of pedotype Budig. Pedotype Budig has the highest Hm / Gt value, indicating such a well-drained environment that waterlogging was low, and the thick Bt horizon of pedotype Budig suggests evident leaching in a humid paleoclimate, for example at level 0–55 m. Pedotype Budig might have good drainage in sandy structure which promotes the transformation of goethite into hematite, leading to the higher value of Hm / Gt. Excluding pedotype Budig, Hm / Gt agrees well with the humidity stages deduced from paleosol units, also providing more detailed variations (Fig. 6g). At level 55–250 m, there is high frequency alternation of waterlogging with a cycle of ~0.1 Ma (Liu et al., 2017), which is followed by a long term semiarid well-drained environments (250–546 m) interrupted by short term humid events (thin sandy layers

and a few gleied paleosols). From level 546 m to 740 m, strong waterlogging becomes dominant until aridity at level 740–755 m with well-drained pedotype Tas.

Note that the variation of Hm / Gt is compatible with other paleoclimatic records. In Xiagou Formation (0–474 m), the high amplitude changes at 55–250 m and low amplitude changes at 250–474 m of magnetic susceptibility (Liu et al., 2017) are similar with patterns of Hm / Gt in these ranges. In addition, the ratio of Hm / Gt indicates a general alternation of waterlogging stages: wet (55–250 m), dry (250–546 m), wet (546–740 m), which were comparable to the results from paleosol units (Fig. 6g) and regional and global oxygen isotope records (Fig. 6k) (Li et al., 2013; Ogg et al., 2016). These agreements on one hand support the magnetic susceptibility chronology of Zhangye Danxia (Liu et al., 2017), and on the other hand, suggests that the paleosol succession in Zhangye Danxia is a detailed record of paleoclimate. Further investigation of this unique section potentially provides more insights of paleoclimate during Aptian and Albian.

5. Conclusions

In this study, we reported a unique succession of Early Cretaceous (Aptian-Albian) paleosols in Zhangye Danxia National Geopark, northwestern China. The paleosols were identified and characterized in field based on pedogenic features such as root traces, soil structures and soil horizons. Paleosol classification and interpretation were achieved by comparison with their modern analogues. In Zhangye Danxia section (755 m thick), 155 paleosol profiles of 14 different pedotypes were identified by field and micromorphology. Most pedotypes or soil units resembled modern soilscapes in South Asia, suggesting more humid and hotter environment than at present. Eleven paleoclimate stages were deduced from systematic analysis of soil units. The paleosol alternation and waterlogging variation based on the ratio of Hm / Gt conforms to regional and global records during Aptian and Albian, which is potentially served for paleoclimate reconstruction.

Declaration of Competing Interest

The authors declare that they have no known competing financial interests or personal relationships that could have appeared to influence the work reported in this paper.

Acknowledgements

We are grateful to the editors and two anonymous reviewers for their constructive comments, which improve the original manuscript greatly. Staffs in Zhangye Danxia National Geopark are appreciated for their supports in the fieldwork. This work is financially supported by Natural Science Foundation of Fujian province (2020J01141), National Natural Science Foundation of China (Grant No. 41602184, 42130507, 41772180), and Innovation Research Team Fund of Fujian Normal University (Grant No. IRTL1705).

References

Brewer, R., 1976. Fabric and mineral analysis of soils. Robert E Krieger Publishing Company, New York.
De Smedt, A., Mostaert, A., 1964. Le dialecte monguor parlé par les Mongols du Kansou occidenta 2 partie grammaire. Mouton, The Hague.
Deaton, B.C., Balsam, W.L., 1991. Visible spectroscopy - a rapid method for determining hematite and goethite concentration in geological materials. J. Sediment. Petrol. 61, 628–632. https://doi.org/10.1306/d4267794-2b26-11d7-8648000102c1865d.
Deng, S., Yang, X., Lu, Y., 2005. Pseudofrenelopsis (Cheirolepidiaceae) from the Lower Cretaceous of Jiuquan, Gansu, northwestern China. Acta Palaeontol. Sin. 44, 505–516.
Ding, H., Wang, S., Yao, X., Kang, L., Yin, Z., Zhang, X., 2014. The geologic origins of Danxia and colorfull hills landform of Zhangye in China. Gansu Geol. 23, 70–77 (in Chinese with English abstract).
Fitzpatrick, E.A., 1984. Micromorphology of soils, second. ed. Chapman and Hall Ltd, London.
Food and Agriculture Organization, 1977. Soil map of the world 1:5000000, VII, South Asia. UNESCO, Paris.
Food and Agriculture Organization, 1978. Soil map of the world 1:5000000, VIII. North and Central Asia, UNESCO, Paris.
Hao, Y., Su, D., Yu, J., Li, Y., Zhang, W., Liu, G.F., 2000. 2000, Stratigraphical Lexicon of China Cretaceous. Geological Publishing House, Beijing.
Harris, J., Lamanna, M., You, H., Ji, S., Ji, Q., 2006. A second enantiornithean (Aves: Ornithothoraces) wing from the Early Cretaceous Xiagou Formation near Changma, Gansu Province, People's Republic of China. Can. J. Earth Sci. 43, 547–554.
Hay, W.W., 2017. Toward understanding Cretaceous climate—An updated review. Sci. China Earth Sci. 60, 5–19. https://doi.org/10.1007/s11430-016-0095-9.
He, H., Wang, X., Zhou, Z., Wang, F., Boven, A., Shi, G., Zhu, R., 2004. Timing of the Jiufotang Formation (Jehol Group) in Liaoning, northeastern China, and its implications. Geophys. Res. Lett. 31, 261–268.
Hu, Y.X., 2004. Early Cretaceous ostracods from the Xiagou formation of Hongliuxia in the Yumen area, Gansu of NW China. Acta Microbiol Sin. 21, 439–455 (in Chinese with English abstract).
Hu, Y., Xu, D.L., 2005. Early Cretaceous ostracods from the Xiagou Formation in Xiagou, Gansu Province. Acta Microbiol Sin. 22, 173–184 (in Chinese with English abstract).
Hu, X., Scott, R.W., Cai, Y., Wang, C., Melinte-Dobrinescu, M.C., 2012. Cretaceous oceanic red beds (CORBs): Different time scales and models of origin. Earth Sci. Rev. 115, 217–248. https://doi.org/10.1016/j.earscirev.2012.09.007.
Hu, P., Liu, Q., Torrent, J., Barrón, V., Jin, C., 2013. Characterizing and quantifying iron oxides in Chinese loess / paleosols : Implications for pedogenesis. Earth Planet. Sci. Lett. 369–370, 271–283. https://doi.org/10.1016/j.epsl.2013.03.033.
Hu, P., Liu, Q., Heslop, D., Roberts, A.P., Jin, C., 2015. Soil moisture balance and magnetic enhancement in loess–paleosol sequences from the Tibetan Plateau and Chinese Loess Plateau. Earth Planet. Sci. Lett. 409, 120–132. https://doi.org/10.1016/j.epsl.2014.10.035.
Huang, C.M., Retallack, G.J., Wang, C.S., 2012. Early Cretaceous atmospheric pCO2 levels recorded from pedogenic carbonates in China. Cretac. Res. 33, 42–49. https://doi.org/10.1016/j.cretres.2011.08.001.
Jenkyns, H.C., 2010. Geochemistry of oceanic anoxic events. Geochem. Geophys. Geosyst. 11, Q03004. https://doi.org/10.1029/2009GC002788.
Ji, J., Balsam, W., Chen, J., Liu, L., 2002. Rapid and quantitative measurement of hematite and goethite in the Chinese loess-paleosol sequence by diffuse reflectance spectroscopy. Clay Clay Miner. 50, 208–216. https://doi.org/10.1346/000986002760832801.
Kraus, M.J., 1999. Paleosols in clastic sedimentary rocks: their geologic applications. Earth Sci. Rev. 47, 41–70.
Leckie, R.M., Bralower, T.J., Cashman, R., 2002. Oceanic anoxic events and plankton evolution: Biotic response to tectonic forcing during the mid-Cretaceous. Paleoceanography 17. https://doi.org/10.1029/2001PA000623, 13–1–13–29.
Lepre, C.J., Olsen, P.E., 2021. Hematite reconstruction of late triassic hydroclimate over the Colorado Plateau. Proc. Natl. Acad. Sci. U. S. A. 118, e2004343118 https://doi.org/10.1073/pnas.2004343118.
Li, H., Yang, J., 2004. Evidence for Cretaceous uplift of the northern Qinghai-Tibetan plateau. Earth Sci. Front. 11, 345–359 (in Chinese with English abstract).
Li, D., Peng, C., You, H., Lamanna, M., Harris, J., Lacovara, K., Zhang, J., 2007. A large therizinosauroid (Dinosauria: Theropoda) from the Early Cretaceous of northwestern China. Acta Geol. Sin. 81, 539–549.
Li, X., Xu, W., Liu, W., Zhou, Y., Wang, Y., Sun, Y., Liu, L., 2013. Climatic and environmental indications of carbon and oxygen isotopes from the Lower Cretaceous calcrete and lacustrine carbonates in Southeast and Northwest China. Palaeogeogr. Palaeoclimatol. Palaeoecol. 385, 171–189. https://doi.org/10.1016/j.palaeo.2013.03.011.
Li, J., Wen, X.Y., Huang, C.M., 2016. Lower Cretaceous paleosols and paleoclimate in Sichuan Basin, China. Cretac. Res. 62, 154–171. https://doi.org/10.1016/j.cretres.2015.10.002.
Li, Y.X., Gill, B., Montañez, I.P., Ma, L., LeRoy, M., Kodama, K.P., 2020. Orbitally driven redox fluctuations during Cretaceous Oceanic Anoxic Event 2 (OAE2) revealed by a new magnetic proxy. Palaeogeogr. Palaeoclimatol. Palaeoecol. 538, 109465 https://doi.org/10.1016/j.palaeo.2019.109465.
Liu, Z.S., 2000. Early Cretaceous sporopollen assemblage from the Hanxia of Yumen in Gansu, NW China. Acta Microbiol Sin. 17, 73–84 (in Chinese with English abstract).
Liu, Q.S., Torrent, J., Barrón, V., Duan, Z.Q., Bloemendal, J., 2011. Quantification of hematite from the visible diffuse reflectance spectrum: effects of aluminium substitution and grain morphology. Clay Miner. 46, 137–147. https://doi.org/10.1180/claymin.2011.046.1.137.
Liu, H., Kuang, H., Hu, X., Liu, Y., Peng, N., Wang, X., Xu, J., Xue, P., Chen, J., 2013. Sedimentary facies of the Lower Cretaceous Xiagou and Zhonggou Formation in Hanxia, northern Qilian Mountain, Gansu province, northwest China. Acta Sedimentol. Sin. 32, 248–258 (in Chinese with English abstract).
Liu, Z., Liu, X., Huang, S., 2017. Cyclostratigraphic analysis of magnetic records for orbital chronology of the Lower Cretaceous Xiagou Formation in Linze, northwestern China. Palaeogeogr. Palaeoclimatol. Palaeoecol. 481, 44–56. https://doi.org/10.1016/j.palaeo.2017.05.022.
Ogg, J.G., Ogg, G.M., Gradstein, F.M., 2016. Cretaceous. In: A Concise Geologic Time Scale, pp. 167–186. https://doi.org/10.1016/B978-0-444-59467-9.00013-3.
Retallack, G., 1984. Completeness of the rock and fossil record: some estimates using fossil soils. Paleobiology 10, 59–78.
Retallack, G.J., 1988. Field recognition of paleosols. In: Reinhardt, J., Sigleo, W.R. (Eds.), Paleosols and Weathering Through Geologic Time: Principles and Applications. Geological Society of America Special Paper, pp. 1–20.
Retallack, G.J., 1994. A pedotype approach to latest Retaceous and earliest Tertiary paleosols in eastern Montana. Geol. Soc. Am. Bull. 106, 1377–1397.

Retallack, G.J., 1997. A Color Guide to Paleosols. John Wiley & Sons Ltd, New York.
Retallack, G.J., 2005. Pedogenic carbonate proxies for amount and seasonality of precipitation in paleosols. Geology 33, 333–336. https://doi.org/10.1130/G21263.1.
Retallack, G.J., 2013. Early cambrian humid, tropical, coastal paleosols from Montana, USA. In: Driese, S.G., Nordt, L.C. (Eds.), New Frontiers in Paleopedology and Terrestrial Paleoclimatology: Paleosols and Soil Surface Analog Systems. SEPM (Society for Sedimentary Geology), pp. 257–272. https://doi.org/10.2110/sepmsp.104.09.
Retallack, G.J., 2016. Field and laboratory tests for recognition of Ediacaran paleosols. Gondwana Res. 36, 94–110. https://doi.org/10.1016/j.gr.2016.05.001.
Retallack, G.J., 2019. Soil of the past. Wiley, Chichester.
Retallack, G.J., Dilcher, D.L., 2012. Core and geophysical logs versus outcrop for interpretation of Cretaceous paleosols in the Dakota Formation of Kansas. Palaeogeogr. Palaeoclimatol. Palaeoecol. 329–330, 47–63.
Retallack, G.J., Huang, C., 2010. Depth to gypsic horizon as a proxy for paleoprecipitation in paleosols of sedimentary environments. Geology 38, 403–406. https://doi.org/10.1130/G30514.1.
Retallack, G.J., Kirby, M.X., 2007. Middle Miocene global change and paleogeography of Panama. Palaios 22, 667–679.
Retallack, G.J., Bestland, E.A., Fremd, T.J., 2000. Eocene and Oligocene paleosols of central Oregon. In: Special Paper of the Geological Society of America, 344, pp. 1–192. https://doi.org/10.1130/0-8137-2344-2.1.
Scheinost, A.C., Schwertmann, U., 1999. Color Identification of Iron Oxides and Hydroxysulfates. Soil Sci. Soc. Am. J. 63, 1463–1471. https://doi.org/10.2136/sssaj1999.6351463x.
Schwertmann, U., 1988. Occurrence and formation of iron oxides in various pedoenvironments. In: Stucki, J.W., Goodman, B.A., Schwertmann, U. (Eds.), Iron in Soils and Clay Minerals. Springer, Dordrecht, pp. 267–308. https://doi.org/10.1007/978-94-009-4007-9_11.
Sheldon, N.D., Retallack, G.J., 2001. Equation for compaction of paleosols due to burial. Geology 29, 247–250. https://doi.org/10.1130/0091-7613(2001)029<0247:EFCOPD>2.0.CO;2.
Sheldon, N.D., Tabor, N.J., 2009. Quantitative paleoenvironmental and paleoclimatic reconstruction using paleosols. Earth Sci. Rev. 95, 1–52. https://doi.org/10.1016/j.earscirev.2009.03.004.
Suarez, M.B., Ludvigson, G.A., González, L.A., Al-Suwaidi, A.H., You, H.-L., 2013. Stable isotope chemostratigraphy in lacustrine strata of the Xiagou Formation, Gansu Province, NW China. Geol. Soc. Lond., Spec. Publ. 382, 143–155. https://doi.org/10.1144/SP382.1.
Sun, B., Du, B., Ferguson, D., Chen, J., He, Y., Wang, Y., 2013. Fossil equisetum from the lower Cretaceous in Jiuquan Basin, Gansu, Northwest China and its paleoclimatic significance. Palaeogeogr. Palaeoclimatol. Palaeoecol. 385, 202–212.
Tabor, N.J., Myers, T.S., 2015. Paleosols as indicators of paleoenvironment and paleoclimate. Annu. Rev. Earth Planet. Sci. 43, 333–361. https://doi.org/10.1146/annurev-earth-060614-105355.
Tate, T., Retallack, G., 1995. The thin section of paleosol. J. Sediment. Res. A65, 579–580.
Vepraskas, M.J., Richardson, J.L., 2000. Wetland soils: genesis, hydrology, landscapes, and classification. CRC Press, Boca Raton.
Wang, Q., Yang, J., Lu, H., 2003. Some Early Cretaceous charophytes from Gaotai county, Gansu of NW China. Acta Micropalaeontologica Sinica 21, 187–198.
Wang, C., Hu, X., Huang, Y., Wagreich, M., Scott, R., Hay, W., 2011. Cretaceous oceanic red beds as possible consequence of oceanic anoxic events. Sediment. Geol. 235, 27–37. https://doi.org/10.1016/j.sedgeo.2010.06.025.
Wang, Y., Sha, J., Pan, Y., Zhang, X., Rai, X., 2012. Non-marine Cretaceous ostracod assemblages in China a preliminary review. J. Sratigr. 36, 290–299.
Wang, C., Feng, Z., Zhang, L., Huang, Y., Cao, K., Wang, P., Zhao, B., 2013. Cretaceous paleogeography and paleoclimate and the setting of SKI borehole sites in Songliao Basin, northeast China. Palaeogeogr. Palaeoclimatol. Palaeoecol. 385, 17–30. https://doi.org/10.1016/j.palaeo.2012.01.030.
Yang, X., Deng, S., 2007. Discovery of Pseudofrenelopsis gansuensis from the Lower Cretaceous of Wangqing, Jilin Province, and its significance in correlation of Cretaceous red beds in China. Acta Geol. Sin. 81, 905–910.
You, H.-L., Li, D.-Q., 2009. The first well-preserved Early Cretaceous brachiosaurid dinosaur in Asia. Proc. R. Soc. B Biol. Sci. 276, 4077–4082. https://doi.org/10.1098/rspb.2009.1278.
You, H., Lamanna, M., Harris, J., Chiappe, L., O'Connor, J., Ji, S., Lü, J., Yuan, C., Li, D., Zhang, X., Lacovara, K., 2006. A nearly modern amphibious bird from the Early Cretaceous of northwestern China. Science 312, 1640–1643.
Zachos, J.C., Dickens, G.R., Zeebe, R.E., 2008. An early Cenozoic perspective on greenhouse warming and carbon-cycle dynamics. Nature 451, 279–283. https://doi.org/10.1038/nature06588.
Zhang, M., Ji, L., Du, B., Dai, S., Hou, X., 2015. Palynology of the Early Cretaceous Hanxia Section in the Jiuquan Basin, Northwest China: The discovery of diverse early angiosperm pollen and paleoclimatic significance. Palaeogeogr. Palaeoclimatol. Palaeoecol. 440, 297–306. https://doi.org/10.1016/j.palaeo.2015.09.010.
Zheng, D., Wang, H., Li, S., Wang, B., Jarzembowski, E.A., Dong, C., Yanan, F., Teng, X., Yu, T., Yang, L., Li, Y., Zhao, X., Xue, N., Chang, S., Zhang, H., 2021. Synthesis of a chrono- and biostratigraphical framework for the Lower Cretaceous of Jiuquan, NW China: Implications for major evolutionary events. Earth Sci. Rev. 213, 103474 https://doi.org/10.1016/j.earscirev.2020.103474.